



Article

Effect of Surface Texturing on Cast Iron Reciprocating against Steel under Cyclic Loading in Boundary and Mixed Lubrication Conditions

Bastian Meylan, Fatemeh Saeidi and Kilian Wasmer * 

Advanced Materials Processing Laboratory, Swiss Federal Laboratories for Materials Science and Technology (Empa), Feuerwerkerstrasse 39, 3602 Thun, Switzerland; bastian.meylan@empa.ch (B.M.); fatemeh.saeidi@empa.ch (F.S.)

* Correspondence: kilian.wasmer@empa.ch; Tel.: +41-58-765-6271

Received: 21 September 2017; Accepted: 25 December 2017; Published: 2 January 2018

Abstract: This study investigates the effect of laser surface texturing on the friction behavior of grey cast iron reciprocating under boundary, mixed lubrication conditions and cyclic loading. Four geometrical parameters of micro-textures (feature depth, feature diameter, area fraction, and sliding direction) were studied using a design of experiments (DoE) approach. The results showed that depending on the geometry, micro-textures can have either a positive or a negative effect on the friction behavior. The DoE analysis revealed that the coefficient of friction is mainly affected by the interaction of the feature depth and its diameter. It was found that this can be related to the aspect ratio of the dimples, and the best results were obtained for an aspect ratio of 0.1 and 0.17.

Keywords: tribology; surface engineering; laser surface texturing; mixed lubrication; starved lubrication; design of experiment

1. Introduction

Nowadays, there is a great need for energy saving and any field related has attracted considerable attention in recent years. For moving systems or systems with moving parts, one way to decrease the energy consumption is to reduce the frictional losses. One of the potential methods to decrease friction is texturing the surface of the moving pieces [1]. Surface texturing consists of producing regular patterns on the surface in order to improve the tribological properties of the pieces [2]. One popular method to produce the structures is by laser machining [2–4]. Indeed, laser surface texturing is a versatile method that allows us to easily create various dimple shape geometries [5,6], depths [7,8], sizes [9,10], or distributions [4,11].

Three main mechanisms have been proposed to explain the better tribological properties of textured surfaces. The first mechanism is an increase of the hydrodynamic pressure due to the micro irregularities of the surface [12,13]. This mechanism was first shown for protruding asperities, but was later also adapted for dimples or negative indents by Etsion and Burstein [14]. This mechanism works in the hydrodynamic regime where no solid contacts take place and this is why positive (protruding) or negative (recessed) texturing can be used. The second mechanism occurs more towards boundary or starved lubrication with dimples. In this case, the dimples can act as oil reservoirs and facilitate the re-lubrication of the surface in starved conditions [15–17]. The last mechanism proposed to improve the properties is the trapping of wear debris inside the dimples [18,19]. This mechanism can be effective both for dry [18,19] and for lubricated conditions [3,10].

The effects of surface texturing have been mostly studied on laboratory standard equipment, such as pin-on disk tribometers [4,8,9,18–20]. These tools are helpful for preliminary investigations and normalized tests, but the direct application of the results to a real mechanical system may be

very hazardous. A few studies have been done on journal bearing but mostly in unidirectional sliding and hydrodynamic conditions [5,7]. In this study, the effect of several texture parameters is investigated in a custom-made, half-journal bearing with reciprocating sliding under complex cyclic loading. This custom made tribo-setup was designed to simulate a half-journal bearing used in an industrial cutting machine.

2. Materials and Methods

2.1. Tribological Setup

The tribological experiments were carried out on a custom-made setup allowing for the reciprocating sliding of a steel axis against a half-journal bearing as shown in Figure 1a. The setup is identical to that used in our previous studies, and all of the details of the machine and test procedure are given in Meylan et al. [21]. This setup is made to simulate the exact contact pressure and reciprocal movement as for a half-journal bearing used in an industrial cutting machine.

During each reciprocating cycle, the load is varied between a minimum (1 or 4 kN) and a maximum load that can go as high as 250 kN according to Figure 1b. Most of the rotation occurs at the minimum load. As the load is increased sharply, the maximum load is reached at the end of the rotation. This maximum load corresponds to a pressure of 110–180 MPa over the contact surface as calculated by Finite Element (FE) simulations (not shown here). Then, the load decreases sharply when the axis is rotated back to its initial position. The number of cycles per hour (cycle rate) can also be adjusted between 3000 and 9500 cycles/h. During the complete duration of a test, a commercial industrial lubricant with a viscosity of 220 cSt. at 40 °C (DIN 51506 VBL) was poured into the gap between the two pieces at a rate of 1.3 ± 0.02 dL/min (See Figure 1a). The oil was applied by gravity. In other words, the oil was dropped into the interstice between the steel and cast iron so that it could flow freely in the contact. The rate was measured several times before and after the experiments to check the variations of the debit.

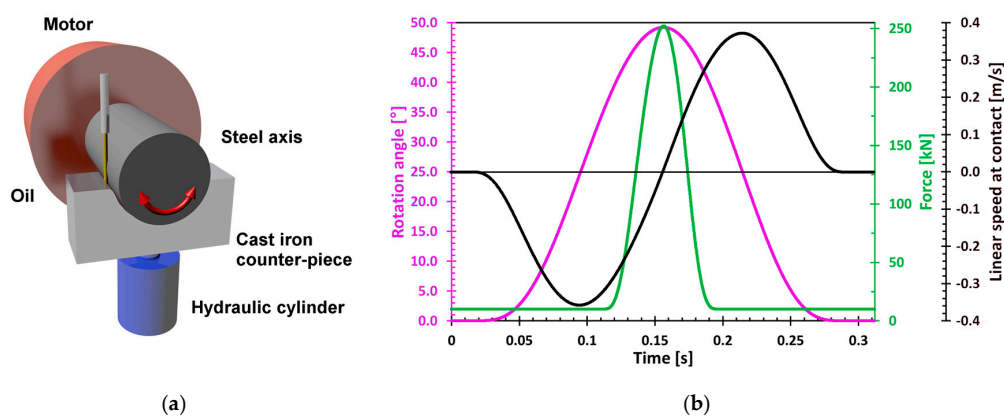


Figure 1. (a) Schematic representation of the tribological setup; (b) Graph showing the reciprocal rotation of the axis (pink), the load applied (green), and the linear speed at the contact (black) for one cycle with a maximum load of 250 kN applied.

The same procedure as in our previous study [21] was used for the running-in to avoid catastrophic failure and is given in Appendix A, Table A1. During the first 8 h of sliding, the load and the cycle rate were progressively increased from 60 to 250 kN and from 4000 to 9500 cycles/h, respectively. After, the loading procedure (8 h), the maximum load, and the cycle rate were kept at their maximum values of 250 kN and 9500 cycles/h, respectively, whereas the minimum load was increased and kept constant to 4 kN for 8 h.

The machine was stopped after 4.5, 8, and 16 h. These stops were necessary to change the settings and to allow for ex situ observations of the surface. Each stop was sufficiently long to cool the machine and the oil down to their initial temperatures before restarting the test.

In our previous study, it was found that the steady-state starts after approximately 10 h. In this study, to be on the safe side and ensure that all of the samples have reached the steady-state for comparison, the tribological properties were compared for the period between 12 and 15 h.

2.2. Design of Experiment (DoE)

Due to the high cost and time needed for each experiment, only a limited number of tests could be planned. Under such circumstances, design of experiment (DoE) methods are very efficient as they allow us to obtain as much information as possible when testing several factors with a limited number of tests. This method requires much less testing than for example testing one factor at a time, and it is also possible to obtain information on the interactions between the factors [21]. Consequently, in order to extract as much information from the limited number of tests, a two-level factorial design was used.

In this study, elongated dimples distributed regularly in a hexagonal matrix were investigated as illustrated in Figure 2a. The dimples are similar to the ones used by Saedi et al. [10,20], and the factors are the same except for the length. Indeed, to reduce the number of tests in this study, the length was kept constant at 500 μm . Four factors were investigated, which are the depth (h), the diameter (d), the area fraction of micro-textures (f), and the sliding direction relative to the major axis of micro-textures (α). The different factors are illustrated in Figure 3, and the values of the two levels used for each factor are shown in Table 1.

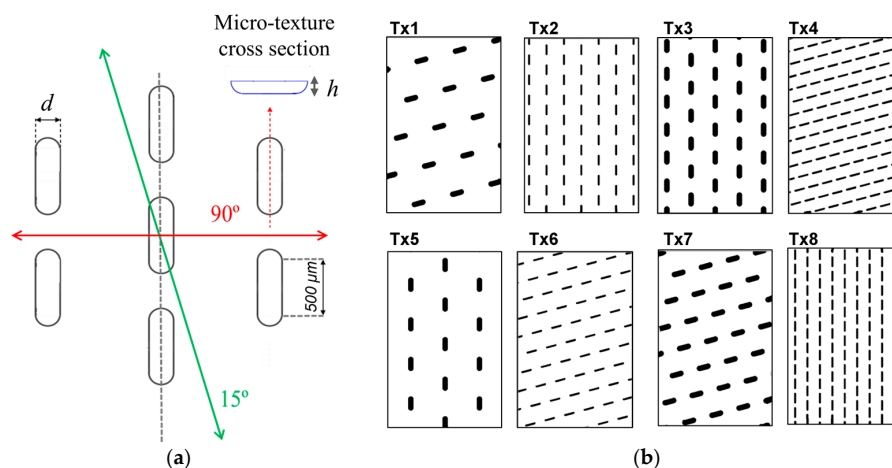


Figure 2. (a) Schematic representation of the geometric parameters used for the Design of Experiment (DoE); (b) Schematic representation of the eight textures generated by the DoE, Tx 1–4 have a depth of 50 μm , whereas Tx 5–8 have a depth of 10 μm .

Table 1. Factors, levels, and coded values of the design of experiments.

Factors	Low Level	High Level
Height (h) (μm)	10	50
Diameter (d) (μm)	100	300
Area fraction (f) (%)	5	10
Sliding direction (α) (deg.)	15	90
Code	−1	1

A full two-level factorial design with four factors still requires 16 experiments ($2^4 = 16$). This was however not possible resource wise, so a fractional factorial design was used [22,23]. One-half fraction,

or 2^{4-1} , was selected in this work, which decreased the number of experiments by a factor 2 and so decreased the number of experiments to eight. The fractional factorial design was defined using the generator $I = hdfa$. This means that each main factor is aliased with the interaction of the three other factors, and that each interaction of two factors is aliased with the interaction of the other remaining two factors. As a consequence, the design is of resolution IV. Resolution IV designs are good for studying the influence of the main factors and interactions of two factors, but are limited to a higher factor as the influence of the interactions are aliased. Equation (1) shows our first-degree polynomial model with interactions:

$$Y = a_0 + a_1h + a_2d + a_1f + a_1\alpha + a_{12}hd + a_{13}hf + a_{14}h\alpha + \varepsilon \quad (1)$$

where Y is the experimental response, a_0 is a constant, a_i are the main effect coefficients associated with the main factors, a_{ij} are the interaction effect coefficients, and ε is the error observed in the response Y (also known as the residual). The other two factors interactions are aliased with those shown in Equation (1). The eight textures generated by the fractional factorial design are shown in Figure 2b and the parameters of the eight structures are summarized in Table 2. To avoid any influence of the order of the experiment, the tests are run in a random order as shown in the second column of Table 2.

Table 2. The run order and surface textures parameters for the eight textures, as well as the values for the main response studied in this work (the average maximum torque between 12 and 15 h sliding).

Texture	Run Order	A: (h) (μm)	B: (d) (μm)	C: (f) (%)	D: (α) ($^\circ$)	Response: Average Maximum Torque (Nm)
Tx 1	5	50	300	5	15	301
Tx 2	8	50	100	5	90	324
Tx 3	1	50	300	10	90	227
Tx 4	4	50	100	10	15	334
Tx 5	3	10	300	5	90	518
Tx 6	7	10	100	5	15	280
Tx 7	6	10	300	10	15	380
Tx 8	2	10	100	10	90	238

2.3. Materials and Sample Preparation

The steel axes of the tribo-system had a diameter of 65 mm and were made of a standard 42CrMoS4 steel with the chemical composition given in Table 3. The surface roughness (Sa) was $0.32 \pm 0.02 \mu\text{m}$. The counter-pieces were in grey cast iron (composition given in Table 3) with an inner diameter of 65.14 mm. All of the surfaces of the grey cast iron workpieces have a surface roughness (Sa) of the contact region of $0.9 \pm 0.1 \mu\text{m}$ after electric discharge machining (EDM).

Table 3. Chemical composition of the grey cast iron samples and the steel axes (wt %).

	C	Mn	Si	P	S	Cu	Cr	Mo	Fe
Grey cast iron	2.890	0.940	1.470	0.036	0.059	1.000	-	-	Balance
42CrMo4 steel	0.400	0.750	0.330	0.035	0.028	-	1.010	0.160	Balance

The textures on the cast iron pieces were machined using a pulsed near-infrared laser with a wavelength of 1064 nm and a pulse duration of 100 ns. The fluence of ablation was 4.2 J/cm^2 . As a consequence, splatters are produced during the ns laser pulses and ejected from the ablation zone. They accumulate around the dimples and form ridges as shown in Figure 3. To avoid any influences of these ridges during the sliding, they were ground out before performing the test. The grinding procedure was stopped before doing any modification to the roughness of the contacting surface.

This is confirmed by the topographic measurements made before and after grinding, and the fact that the roughness between the dimples is intact (see Figure 3).

In addition to the textured samples, seven samples without texture were also evaluated as reference surfaces in order to provide a comparison with the textured samples. The reference samples have the same surface topography as the region between the dimples of the textured samples (see Figure 3).

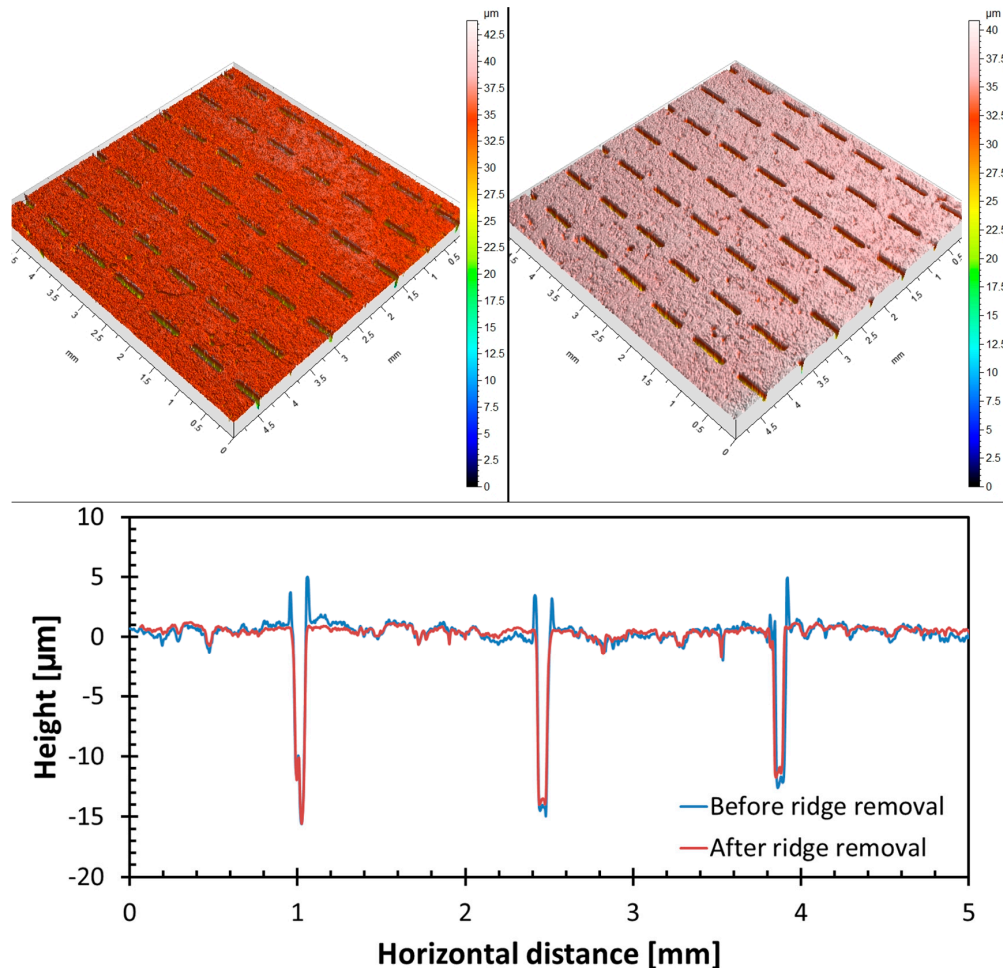


Figure 3. Topography measurement of the surface Tx 8 directly after laser processing (**left**) and after grinding the ridges around the dimples (**right**). Comparison of the profiles shows the disappearance of the ridges after grinding. The surfaces are shown after the removal of the cylindrical form of the cast iron piece.

2.4. Ex Situ Characterisation of the Surface

As previously mentioned, the cast iron counter-pieces were dismantled after 4.5, 8, and 16 h for ex situ observation. To start with, a visual observation of the surface was made to ensure that no severe wear had occurred during testing. Secondly, the surface was cleaned with acetone followed by ethanol in an ultrasonic bath. Then, the surfaces' topography was measured with a white light profilometer Altisurf 500 from Altimet (Evian, France) that was equipped with an optical pen OP300WM from Stil SA. The given specifications are a maximum vertical range of 300 μm and an axial resolution of 10 nm. Surfaces of $5 \times 5 \text{ mm}^2$ were scanned with a lateral step of 5 μm similar to the maps shown in Figure 3.

3. Results

3.1. Tribological Tests

The evolution of the maximum torque with the corresponding sliding time is shown for three selected textured samples in Figure 4a. In this figure, only the textures with the maximum effects are shown since the others are close to the reference sample which makes the graph difficult to read (see Figure 4b). In addition, the average of the seven reference samples with their corresponding standard deviation is also shown in this figure for comparison. During the two stages of running-in from 0 to 4.5 h and 4.5 to 8 h, the tribological behavior of the different samples cannot be separated. They roughly follow the same trend and some curves cross each other several times meaning that it is difficult to say which sample performs better during this time. However, clear differences between the samples appear after 8 h when the process parameters are kept constant with the maximum load at 250 kN, the minimum load at 4 kN, and the cycle rate at 9500 cycles/h. From this time, a distinct difference in the maximum torque can be observed between the samples. The torque first increases during the 8 to 12 h period. This is related to an increase of the temperature of the system, and especially the contact and oil temperatures (see Figure A1 in Appendix A). An increase of the oil temperature decreases its viscosity and thus decreases its load carrying capacity, which leads to more solid–solid contacts leading to an increased coefficient of friction. At 12 h, the temperature starts to reach an equilibrium and the maximum torque tends to stabilize for most samples. For texture Tx 5, the behavior between 8 to 12 h is unstable. The torque increases much more at the beginning than all the other samples but decreases sharply at 9 h. This is followed by another increase at 11 h to finally stabilize after 12 h at a very high value. The behavior of Tx 4 is also unstable between 8 and 10 h, but after this time it went back to a normal behavior and so the torque value measured during 12 to 15 h was not affected by these instabilities.

For these reasons, the samples were compared during the 12 to 15 h period where the torque reaches a steady-state and the difference between the samples is maximum. The average maximum torque for the textured samples between 12 and 15 h is summarized in Table 2 and the non-textured reference samples are given in Table 4.

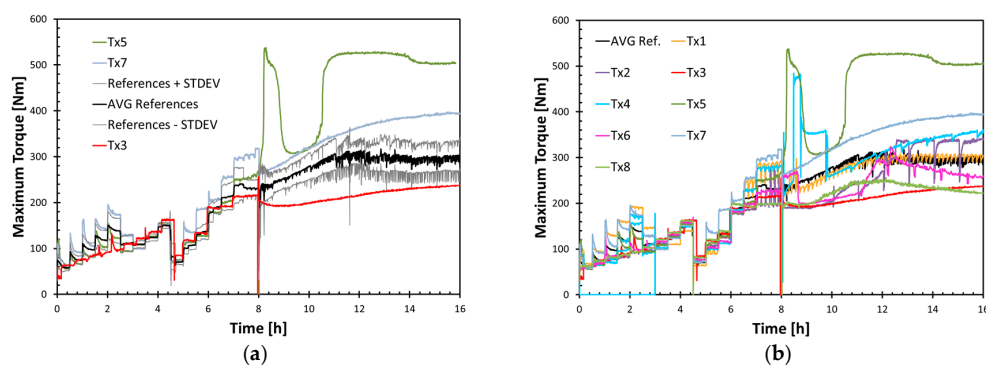


Figure 4. (a) Evolution with time of the maximal torque values for three different textured samples (green, blue, and red lines) compared with the average of the seven reference samples (black line) with ± 1 standard deviation (grey lines); (b) Evolution of the maximal torque values for the eight textured samples compared with the average of the seven reference samples (black line).

Table 4. Average maximum torque between 12 h and 15 h for the reference samples (non-textured).

Reference Sample	1	2	3	4	5	6	7	Average	St. Dev.
Average maximum torque (Nm)	294	257	269	342	288	295	333	297	34

A comparison between the reference samples and the textured samples shows a larger scatter of the data for the textured samples. Indeed, based on Table 2, the average of the eight textured samples is 325 Nm with a standard deviation of 81 Nm whereas the average is 297 ± 34 Nm for the reference samples. As the averages values are within standard deviations, an *F*-test is required to see whether this difference is real or only an artifact. The *F*-test confirmed that there is a 97.5% chance that the influence of the textures is significant. The average of the samples is very close as some textured samples have a lower value than the reference (see Tx 3 and Tx 8 in Figure 4), and some textured samples have a much higher value than the references (see Tx 5 and Tx 7 in Figure 4).

3.2. Statistical Model

As seen in Section 3.1, the different textures have a clear influence on the tribological behavior of the samples. Using linear regression, the coefficients (also known as half-effects) of Equation (1) were calculated and are shown in Table 5. It can be seen that the main coefficient is the interaction between *h* and *d*, followed by the first three main factors (*h*, *d*, and *f*).

Table 5. Coefficients calculated for the complete model shown in Equation (1).

Coefficient	a_0	a_1	a_2	a_3	a_4	a_{12}	a_{13}	a_{14}
Value	325	−29	31	−30	1.5	−64	14	−23

As a first selection, only the fourth-highest terms were kept, and to characterize their significance, a statistical approach based on the analysis of variance (ANOVA) was employed similar to Saeidi et al. [10]. Based on this approach, the only significant term was the interaction, *hd*, between the height and the diameter. The three main factors: height (*h*), diameter (*d*), and area fraction (*f*) are not statistically significant. The ANOVA table is given in Table 6, where *DF* is the degree of freedom and the *F*-value is given by Equation (2):

$$F = \frac{MS_{term}}{MS_{residual}}, \quad (2)$$

where the mean square of terms (MS_{Terms}) is the ratio of the sum of squares within terms to its degree of freedom (SS_{Terms}/DF_{Term}), and similarly ($MS_{Residual} = SS_{Residual}/DF_{Residual}$). The *p*-value is the probability that a given *F*-value is due to noise. A term with a value lower than 5% is considered significant whereas a term with a *p*-value higher than 10% is considered not significant [22]. As can be seen in our model, only the interaction *hd* is significant, but doing a model only with this interaction is a misleading representation of the data. Hence, we decided to keep the next three main factors *h*, *d*, and *f* in the final model.

Table 6. Analysis of variance (ANOVA) for the average maximum torque.

Source	Sum of Squares	DF	Mean Square	F-Value	p-Value Prob > F
Model	54,379.50	4	13,594.88	7.09	0.0697
<i>h</i>	6612.50	1	6612.50	3.45	0.1602
<i>d</i>	7812.50	1	7812.50	4.08	0.1368
<i>f</i>	7442.00	1	7442.00	3.88	0.1434
<i>hd</i>	32,512.50	1	32,512.50	16.96	0.0259
Residual	5750.00	3	1916.67		
Total	60,129.50	7			

The final Equation modeling the average torque is thus given by:

$$\text{Average maximum torque} = 325 - 29 \cdot h + 31 \cdot d - 30 \cdot f - 64 \cdot hd. \quad (3)$$

The R -square value (R^2), Adjusted- R^2 , and Predicted- R^2 of this model are 0.90, 0.78, and 0.32, respectively. This model is relatively accurate for navigating within the existing data, but cannot be used reliably to predict non-existing data or great care has to be taken when doing so. This is probably due to the low number of tests, meaning that one strange experiment, such as for example the Tx 5 shown in Figure 4, can affect to some extent the precision of the model.

3.3. Topographical Evolution

In Figure 5, the evolution of the topography is shown for two textured samples (Tx 3 and Tx 5). On the left, the topography maps show the surface state just before the start of the tribological tests (after texturing and after grinding of the ridges). The laser dimples are well-visible for the 50- μm -deep texture (Figure 5a), and are less marked for the textures with a 10 μm depth (Figure 5c). The surface between the laser dimples is rather rough, as the references were chosen to have a rough surface to avoid scuffing. The surfaces consist of many small craters just a few microns deep with small hills in between. Some craters nevertheless have a comparable depth to the shallow laser dimples ($\sim 10 \mu\text{m}$) (Figure 5c). The craters are also smaller in size than the laser dimples.

After 16 h of sliding, the surfaces have not changed drastically (see Figure 5b,d). Indeed, the wear occurred only on the highest peaks of the surfaces. The small craters of the original surface are still preserved as well as the larger laser dimples.

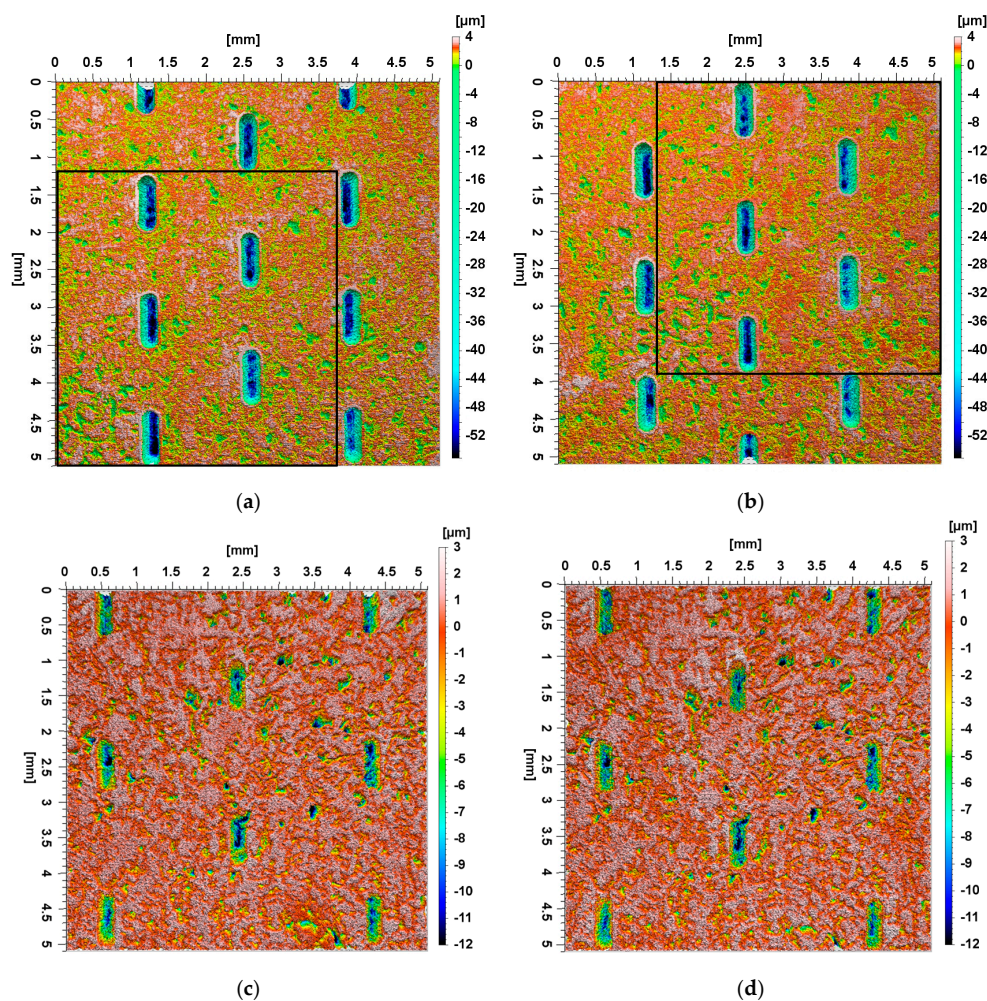


Figure 5. The $5 \times 5 \text{ mm}^2$ topography maps of the surface for sample (a) Tx 3 before sliding; (b) Tx 3 after 16 h of sliding; (c) Tx 5 before sliding; and (d) Tx 5 after 16 h of sliding. Unfortunately, the region of measurements in (a,b) is slightly shifted; the black box indicates the common area.

4. Discussion

Most of the research on the influence of surface texturing have demonstrated an improvement of the tribological properties [1–3], but this is not always the case as reviewed by Gachot et al. [24]. Our results are consistent with Gachot et al. [24], since in our setup and for the selected textures, we observed almost no influence for most surface textures as compared to non-textured samples and an increase of the friction force for two textures and a decrease of the friction for the last two textures. Several factors can be responsible for such behavior. First, the reference surfaces were not perfectly flat but were rough with already a kind of random texturing of the surface. This is well-visible in Figure 5 where small craters are evident on the surfaces. These craters are smaller in size as compared to the big laser textures shown in Figure 5a, but their sizes are not negligible in comparison to the smaller structures shown in Figure 5c. Hence, it is obvious that the tribological performance of the reference surface is already good, and most of the surface textures selected could either have little or not improve it further.

Secondly, some works have already shown the negative influence of surface texturing under starved or boundary conditions [25–27]. Indeed, Podgornik et al. [25] found that under starved lubrication conditions, large dimples can be an obstacle to sliding motion. The dimples are also thought to impact the local stress distribution, meaning a higher load in the region surrounding the dimples, which can lead to an increase of the friction [25,27]. Consequently, the area fraction (f) as well as the size of the dimples (d and h) must be kept below a certain value. In this study, the area fraction (f) was kept low—between 5 and 10%—in order to avoid this problem. Another mechanism explaining the negative impact of dimples under starved lubrication conditions is that the dimples can ultimately become “micro-traps” for oil [26,28]. In other words, the oil in the contact becomes very scarce since it can be trapped in partially empty dimples instead of acting as lubricant in the contact area [28].

In this contribution, it is very likely that the critical moment of the sliding is at the start of the back rotation. The reason is that towards the end of the movement, the load has the highest value when the movement stops, meaning that the system is in boundary or starved conditions. The high pressure at this moment, between 110 and 180 MPa, pushes the oil out of the contact area and as the pieces deform the whole cast iron surface is in contact with the steel, with no gap for oil to enter from the sides. Under these conditions, it is likely that we encounter some of the detrimental effects of the dimples cited in the previous paragraph.

Due to the relatively low number of tests performed, the statistical model proposed has some limitations and should be used within the structures tested. However, interesting information can be obtained when looking at the main factors influencing the average maximum torque. Actually, the only statistically significant term is the interaction between the height and the diameter, hd . As we used a design with a resolution of IV, this term is aliased with the interaction of the two other coefficients, area fraction and sliding direction, f and α . However, the physical meaning of this interaction makes much less sense than hd . The interaction between h and d can be interpreted as the aspect ratio of the dimple h/d . This parameter was already found to play an important role in the improvement of friction [2,4,29–31]. Based on the work of Etsion [3,31] and other researchers [24,32], it was concluded that the h/d ratio is highly dependent on the operating conditions and should be optimized for each set of conditions. In contrast, Schneider et al. [4] found an optimum for the aspect ratio close to 0.1. In this work, the model predicts a lower friction if the height and the diameter are both at the low or high values, respectively. Using our textured geometries, the aspect ratio is either $50/300 \approx 0.17$ or $10/100 = 0.1$. These values correspond well with the one reported by Schneider et al. [4]. On the other hand, when one of the factors is at a low value and the other is at high value, this gives either a low aspect ratio of $10/300 \approx 0.03$ or a high aspect ratio of $50/100 = 0.5$. All of the structures with a small or high aspect ratio performed worse than the one with an aspect ratio close to 0.1. The influence of the aspect ratio is linked in the literature to the capacity of creating fluid vortex in the dimples that effectively creates a shear force and leads to a decrease of the global friction [25]. This mechanism also

competes with the previously mentioned mechanisms that can hinder the tribological properties and so leads to this optimum aspect ratio around 0.1 [4].

The other terms in our model are not statistically significant; this is partially due to the low number of tests and on the other hand can also be a consequence of the interval chosen for the parameters. As explained above, for example, the textured area fraction was kept relatively low—between 5–10%—since this is an interval often cited in the literature as a good interval for surface texturing [33]. It is possible that within the interval chosen, the friction is close to an optimum and so does not vary significantly with the area fraction. It is very probable that if this interval was extended, a larger influence could be detected as it is often reported that the friction decreases for an area fraction that is too high [4].

Finally, the observations of the topography changes before and after the test confirm that the wear during the 16 h of sliding is concentrated on the highest peaks of the surface. These observations confirm our previous findings of the wear evolution of the reference surface [21]. Essentially, the topographical changes occurred mostly at the top of the asperities whereas the craters of the original surfaces and the laser dimples are not affected by the wear. As the wear for these experiments is low, it is not possible to observe a significant difference in the wear rate between the samples. To see an influence, a much longer running time should be used. Another solution could be to use harsher conditions to accelerate the wear rate. One possible solution for this custom-made tribometer would be to increase the minimum load that is applied during most of the stroke. For the current tribo-meter, the maximum load and the cycle rate cannot be increased but there is a potential to increase the minimum load up to 20 kN. Under these conditions, differences in the wear rate for the different textures might be more distinct.

5. Conclusions

In this study, the tribological behavior of textured cast iron samples was investigated under reciprocating sliding and cyclic loading. The cast iron pieces were sliding against a hardened steel axis under mixed and boundary lubrication. The conditions were as close as possible to industrial conditions and so it was not possible to conduct many tests. Because of this, a design of experiment approach was employed. It was found that most of the textures have similar or worse tribological properties than the reference surface without laser texture. This can be explained by the fact that the reference surface is rough and has already micro-craters scattered on the surface. Therefore, the tribological behavior of this reference surface was already good. Also, under starved lubrication conditions, the textures can have a negative influence on the tribological properties due to oil trapping or an increase of local pressure.

Among the studied geometric parameters of the dimples, a semi-empirical model was given that has to be used within the dimples geometry used. It was found that the interaction between the height (h) and the diameter (d) of dimples is the only statistically significant factor influencing the tribological properties. This can be related to the effect of the aspect ratio (h/d) on the tribological properties. The optimal aspect ratio was found to be between 0.1 and 0.17. Too low or too high aspect ratios lead to an increase in friction.

Acknowledgments: The authors would like to thank the Swiss Commission for Technology and Innovation (CTI —project No. 12358.1 PFIW-IW) and the industrial partners for the financial support of this work. Special thanks to Sergio Graca for his assistance in the early stage of this work and Peter Ramseier for his help with the topographic measurements.

Author Contributions: The three authors conceived and designed the experiments together; Bastian Meylan performed the experiments; Bastian Meylan and Fatemeh Saeidi analyzed the data; and Bastian Meylan wrote the paper. Fatemeh Saeidi and Kilian Wasmer participated in scientific discussions, revised the paper, and wrote part of the discussion.

Conflicts of Interest: The authors declare no conflict of interest.

Appendix A

Table A1. Complete experimental conditions used for all of the samples.

	Step Number	Maximum Load (kN)	Minimum Load (kN)	Cycle Rate (cycles/h)	Time (min)
Running-in 1 (4.5 h)	1	60	1	4000	30
	2	90	1	4000	30
	3	120	1	4000	30
	4	150	1	4000	30
	5	180	1	4000	30
	6	150	1	5000	30
	7	120	1	6500	30
	8	100	1	8000	30
	9	100	1	9500	30
Running-in 2 (3.5 h)	10	90	1	4000	30
	11	150	1	5500	30
	12	180	1	6500	30
	13	200	1	9500	30
	14	225	1	9500	30
	15	250	1	9500	60
Steady-state (8 h)	16	250	4	9500	480

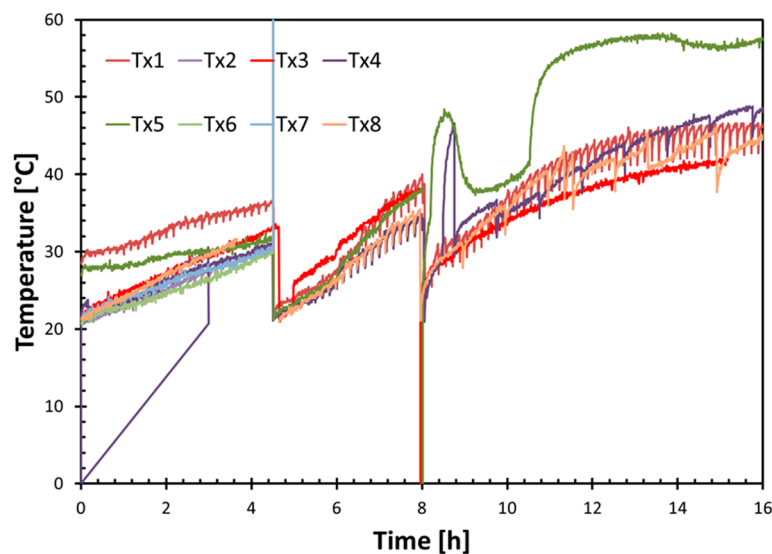


Figure A1. Evolution of the temperature during the tests of different structures. The temperature was measured on the cast iron piece at 5 mm of the contact by a thermocouple.

References

1. Ronen, A.; Etsion, I.; Kligerman, Y. Friction-reducing surface-texturing in reciprocating automotive components. *Tribol. Trans.* **2001**, *44*, 359–366. [[CrossRef](#)]
2. Lu, P.; Wood, R.J.K.; Gee, M.G.; Wang, L.; Pflöging, W. The Friction Reducing Effect of Square-Shaped Surface Textures under Lubricated Line-Contacts—An Experimental Study. *Lubricants* **2016**, *4*, 26. [[CrossRef](#)]
3. Etsion, I. State of the art in laser surface texturing. *Trans. ASME-F-J. Tribol.* **2005**, *127*, 248–253. [[CrossRef](#)]
4. Schneider, J.; Braun, D.; Greiner, C. Laser Textured Surfaces for Mixed Lubrication: Influence of Aspect Ratio, Textured Area and Dimple Arrangement. *Lubricants* **2017**, *5*, 32. [[CrossRef](#)]
5. Yu, H.; Deng, H.; Huang, W.; Wang, X. The effect of dimple shapes on friction of parallel surfaces. *Proc. Inst. Mech. Eng. Part J J. Eng. Tribol.* **2011**, *225*, 693–703. [[CrossRef](#)]

6. Qiu, M.; Minson, B.R.; Raeymaekers, B. The effect of texture shape on the friction coefficient and stiffness of gas-lubricated parallel slider bearings. *Tribol. Int.* **2013**, *67*, 278–288. [[CrossRef](#)]
7. Lu, X.; Khonsari, M.M. An experimental investigation of dimple effect on the stribeck curve of journal bearings. *Tribol. Lett.* **2007**, *27*, 169–176. [[CrossRef](#)]
8. Segu, D.Z.; Choi, S.G.; Choi, J.H.; Kim, S.S. The effect of multi-scale laser textured surface on lubrication regime. *Appl. Surf. Sci.* **2013**, *270*, 58–63. [[CrossRef](#)]
9. Wang, X.; Liu, W.; Zhou, F.; Zhu, D. Preliminary investigation of the effect of dimple size on friction in line contacts. *Tribol. Int.* **2009**, *42*, 1118–1123. [[CrossRef](#)]
10. Saeidi, F.; Meylan, B.; Hoffmann, P.; Wasmer, K. Effect of surface texturing on cast iron reciprocating against steel under starved lubrication conditions: A parametric study. *Wear* **2016**, *348*, 17–26. [[CrossRef](#)]
11. Galda, L.; Pawlus, P.; Sep, J. Dimples shape and distribution effect on characteristics of Stribeck curve. *Tribol. Int.* **2009**, *42*, 1505–1512. [[CrossRef](#)]
12. Hamilton, D.B.; Walowit, J.A.; Allen, C.M. A theory of lubrication by microirregularities. *Trans. ASME J. Basic Eng.* **1966**, *88*, 177–185. [[CrossRef](#)]
13. Anno, J.N.; Walowit, J.A.; Allen, C.M. Microasperity lubrication. *J. Lubr. Technol.* **1968**, *90*, 351–355. [[CrossRef](#)]
14. Etsion, I.; Burstein, L. A model for mechanical seals with regular microsurface structure. *Tribol. Trans.* **1996**, *39*, 677–683. [[CrossRef](#)]
15. Steinhoff, K.; Rasp, W.; Pawelski, O. Development of deterministic-stochastic surface structures to improve the tribological conditions of sheet forming processes. *J. Mater. Process. Technol.* **1996**, *60*, 355–361. [[CrossRef](#)]
16. Lo, S.W.; Horng, T.C. Lubricant permeation from micro oil pits under intimate contact condition. *J. Tribol.* **1999**, *121*, 633–638. [[CrossRef](#)]
17. Fowell, M.; Olver, A.V.; Gosman, A.D.; Spikes, H.A.; Pegg, I. Entrainment and inlet suction: Two mechanisms of hydrodynamic lubrication in textured bearings. *J. Tribol.* **2007**, *129*, 336–347. [[CrossRef](#)]
18. Rosenkranz, A.; Reinert, L.; Gachot, C.; Mucklich, F. Alignment and wear debris effects between laser-patterned steel surfaces under dry sliding conditions. *Wear* **2014**, *318*, 49–61. [[CrossRef](#)]
19. Borghi, A.; Gualtieri, E.; Marchetto, D.; Moretti, L.; Valeri, S. Tribo-logical effects of surface texturing on nitriding steel for high-performance engine applications. *Wear* **2008**, *265*, 1046–1051. [[CrossRef](#)]
20. Saeidi, F.; Parlinska-Wojtan, M.; Hoffmann, P.; Wasmer, K. Effects of laser surface texturing on the wear and failure mechanism of grey cast iron reciprocating against steel under starved lubrication conditions. *Wear* **2017**, *386–387*, 29–38. [[CrossRef](#)]
21. Meylan, B.; Dogan, P.; Sage, D.; Wasmer, K. A simple, fast and low-cost method for in situ monitoring of topographical changes and wear rate of a complex tribo-system under mixed lubrication. *Wear* **2016**, *364*, 22–30. [[CrossRef](#)]
22. Montgomery, D.C. *Design and Analysis of Experiments*, 7th ed.; John Wiley & Sons, Ltd.: London, UK, 2009.
23. Hinkelmann, K.; Kempthorne, O. *Factorial Experiments: Basic Ideas. Design and Analysis of Experiments*; John Wiley & Sons, Inc.: New York, NY, USA, 2007; pp. 419–495.
24. Gachot, C.; Rosenkranz, A.; Hsu, S.M.; Costa, H.L. A critical assessment of surface texturing for friction and wear improvement. *Wear* **2017**, *372*, 21–41. [[CrossRef](#)]
25. Podgornik, B.; Vilhena, L.M.; Sedlacek, M.; Rek, Z.; Zun, I. Effectiveness and design of surface texturing for different lubrication regimes. *Meccanica* **2012**, *47*, 1613–1622. [[CrossRef](#)]
26. Gu, C.X.; Meng, X.H.; Xie, Y.B.; Yang, Y.M. Effects of surface texturing on ring/liner friction under starved lubrication. *Tribol. Int.* **2016**, *94*, 591–605. [[CrossRef](#)]
27. Pettersson, U.; Jacobson, S. Friction and wear properties of micro textured DLC coated surfaces in boundary lubricated sliding. *Tribol. Lett.* **2004**, *17*, 553–559. [[CrossRef](#)]
28. Ryk, G.; Kligerman, Y.; Etsion, I. Experimental investigation of laser surface texturing for reciprocating automotive components. *Tribol. Trans.* **2002**, *45*, 444–449. [[CrossRef](#)]
29. Shinkarenko, A.; Kligerman, Y.; Etsion, I. The effect of surface texturing in soft elasto-hydrodynamic lubrication. *Tribol. Int.* **2009**, *42*, 284–292. [[CrossRef](#)]
30. Kim, B.; Chae, Y.H.; Choi, H.S. Effects of surface texturing on the frictional behavior of cast iron surfaces. *Tribol. Int.* **2014**, *70*, 128–135. [[CrossRef](#)]
31. Etsion, I.; Kligerman, Y.; Halperin, G. Analytical and experimental investigation of laser-textured mechanical seal faces. *Tribol. Trans.* **1999**, *42*, 511–516. [[CrossRef](#)]

32. Qiu, Y.; Khonsari, M. Experimental investigation of tribological performance of laser textured stainless steel rings. *Tribol. Int.* **2011**, *44*, 635–644. [[CrossRef](#)]
33. Wang, X.L.; Kato, K.; Adachi, K.; Aizawa, K. Loads carrying capacity map for the surface texture design of SiC thrust bearing sliding in water. *Tribol. Int.* **2003**, *36*, 189–197. [[CrossRef](#)]



© 2018 by the authors. Licensee MDPI, Basel, Switzerland. This article is an open access article distributed under the terms and conditions of the Creative Commons Attribution (CC BY) license (<http://creativecommons.org/licenses/by/4.0/>).